

# Dynamic Temperature Prediction for the Charging Process of the Fixed Chamber

Yi Zhang<sup>1</sup>, Yan Gao<sup>1</sup>, Zhipeng Xu<sup>1</sup>, Gaoming Zhang<sup>1</sup>, Bin Zhou<sup>1</sup>, Yupei Zhang<sup>2</sup>, Liang Hu<sup>3</sup>

<sup>1</sup> Key Laboratory of In-situ Measurement of Ministry of Education, China Jiliang University, Hangzhou, China  
ilyx\_11@qq.com; gaoyan@cjlu.edu.cn; xuzhipeng@cjlu.edu.cn; zhanggaoming@cjlu.edu.cn; zhoubin@cjlu.edu.cn

<sup>2</sup>Zhejiang Institute of Quality Sciences, Hangzhou, China  
zqs\_zhangyupei@qq.com

<sup>3</sup>State Key Laboratory of Fluid Power and Mechatronic Systems, Zhejiang University, Hangzhou, China  
cmeehuli@zju.edu.cn

**Abstract** – The dynamic gas flow verifier based on the rate of rise (RoR) method is employed for the in-situ calibration of mass flow controllers (MFC) in semiconductor manufacturing. Due to the complicated flow field distribution after process gas charging and the hysteresis characteristics of temperature sensors, accurate average temperature is nearly impossible to measure, and that will significantly affect the accurate metering of the flow rate. Thus, the dynamic temperature prediction based on CFD was proposed to achieve the virtual measurement of the average temperature of the chamber. Then, the dynamic temperature change for different process gases and flow rate was obtained to compensate flow rate calculation. Finally, the experimental apparatus was built up, and detailed comparison was carried out. Results show that the proposed dynamic temperature prediction could satisfy the in-situ verification of the MFCs, the accuracy is approximately  $\pm 0.5\%$  with the flow rate ranging from 5 to 2850 sccm.

**Keywords:** gas flow; in-situ calibration; charging; rate of rise; temperature prediction

## 1. Introduction

Semiconductors are playing increasingly important roles in electronic technology, information technology, communication engineering, solar photovoltaic, medical facility and so on (Ordu 2023) <sup>[1]</sup>. In semiconductor manufacturing, numerous MFCs are employed to provide process gases with a definite flow rate [2, 3]. These MFCs need to be frequently calibrated in-situ to ensure the stability of processing quality. Typically, the gas flow verifier for semiconductor process gas is based on the dynamic pVTt (pressure, volume, temperature, time) method [4]. However, the temperature inside the container is spatially non-uniform, and the difficulty lies in determining the average gas temperature [5, 6]. To calculate the average gas temperature of a 26 m<sup>3</sup> pVTt, Johnson Aaron N. et al. developed a volume-weighted trapezoidal integration procedure using 35 thermistors. The mean gas temperature could be determined with a standard uncertainty of 89 mK and the flow uncertainty in the static pVTt system decreased from 0.22% to 0.13%. J.D. Wright et al. [6, 7] conducted a thermodynamic analysis on a 34 L collection tank based on the RoR method. A lumped parameter model was presented to predict the temperature difference between gas in the tank and water bath. The flow uncertainty was less than 0.12 % for flows from 1 to 200 sccm. At lower and higher flows, the uncertainty increased to about 1% due to leaks and temperature rise resulted from flow work. Primož Žibret et al. [8] proposed an analytical model to calculate the temperature distribution inside the cylinder of a pVTt standard. Results showed that the errors between the dynamic and static methods were reduced to 0.3% by temperature correction. However, the model neglected heat convection inside the cylinder, and the accuracy of the model at high flow rates had to be validated.

In this work, to avoid the long stabilization time of the in-situ gas flow verifier, a dynamic temperature prediction method for the charging process of the chamber based on the RoR dynamic pVTt method is proposed. A 3D CFD simulation was conducted with the flow rate ranging from 5 to 2850 sccm. Moreover, to improve the feasibility of the model, the difference between the average gas temperature and the wall temperature was fitted as a function of flow rate. Finally, the error between the gas verifier and a flow standard was calculated to verify the effectiveness of the proposed method.

## 2. METHODS AND PROCEDURES

### 2.1. Description of the gas flow verifier

Fig. 1 displays the picture and the schematic of the measurement system of the gas flow verifier. The gas flow verifier consists of a standard container of 2.83 L, a sonic nozzle, a vacuum pump, three temperature sensors, a vacuum gauge, and some valves. The sonic nozzle is installed on the upstream side of the standard container to generate critical gas flow and decouple the measurement downstream from the upstream. The vacuum pump is installed at the downstream side of the standard container to control the initial pressure and provide critical flow condition. Temperature sensors T1 and T2 are used to measure the top and side walls of the container, and the temperature sensor T3 is used to measure the temperature at the inlet of the nozzle. The vacuum gauge is used for real-time measurement of pressure inside the standard container. During the calibration, the gas flow verifier is mounted at the downstream side of MFCs to be calibrated. A high precision FLUKE Molbloc/molbox1 gas flow standard with expanded uncertainty of 0.2% is used to validate the accuracy of the gas flow verifier.

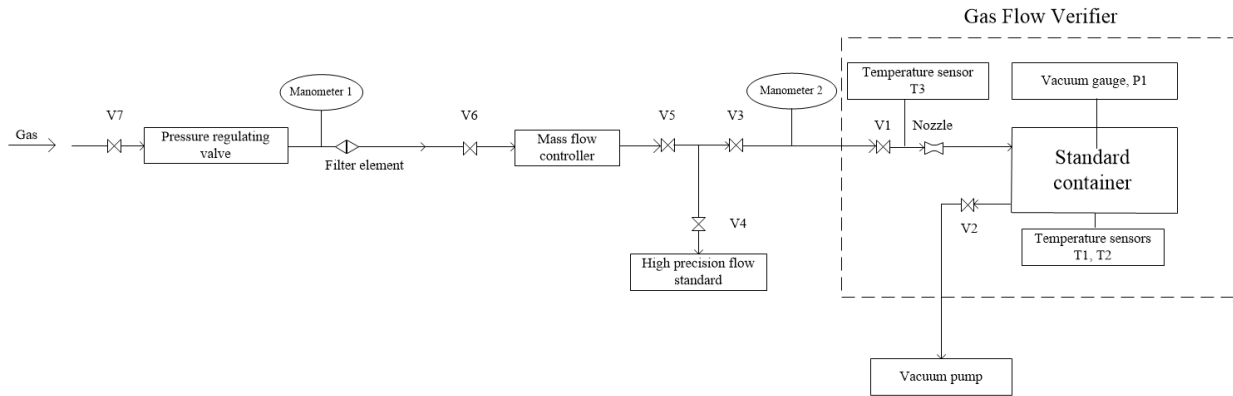


Fig. 1: Schematic of the in-situ verifier.

The implementation of the measurement system of the gas flow verifier is explained as follows:

Firstly, the vacuum pump is started, valve V4 is closed and other valves are opened, which makes sure the container and the pipeline are filled with the gas to be measured.

Secondly, the flow rate of MFC is set, valve V1 is closed and the pressure inside the container decreases to create critical flow. Once the pressure inside the container reaches the set value as shown in Table 1, the valve 2 is closed and the vacuum pump is stopped.

Subsequently, valve V1 is opened and the gas flows through the nozzle and accumulates in the container.

Finally, with an increase in the pressure inside the container, the critical flow condition is not satisfied, and the measurement is finished. During the whole procedure, temperature and pressure are measured continuously.

Table 1: The initial pressure for different flow rate

Flow rates (sccm)	Initial pressure (Pa)
5	66.7
25	124.0
150	346.6
225	367.3
275	411.6
325	484.0
750	832.2
1350	1363.4
1950	1909.2
2850	2643.8

## 2.2. Modelling of the gas flow verifier

Based on the state equation of idea gas, the mass of gas can be calculated as follows:

$$m = \frac{V p}{R_g T_g} \tag{1}$$

where  $m$  is the mass of the gas,  $V$  is the volume of the standard container,  $R_g$  is the specific gas constant,  $p$  is the pressure inside the standard container, and  $T_g$  is the temperature of the gas inside the standard container.

To take the derivative of both sides of equation (1) with respect to time, the mass flow rate of gas can be obtained:

$$\frac{dm}{dt} = \frac{V}{R_g T_g} \frac{dp}{dt} - \frac{pV}{R_g T_g^2} \frac{dT_g}{dt} \tag{2}$$

where  $t$  is time.

From equation (2), real-time pressure and temperature have to be measured to calculate the mass flow rate of gas. Basically, pressure inside the standard container is uniform and measured to calculate rate of pressure rise, which is taken as one of the inputs of the model. However, the temperature inside the standard container is spatial non-uniform and the average gas temperature is not easy to determine. To solve this problem, a three-dimensional CFD simulation of the gas flow verifier is carried out.

## 2.3. 3D CFD simulation of the gas flow verifier

Based on the proposed gas flow verifier, a CFD unsteady simulation is conducted in ANSYS FLUENT to obtain the real-time pressure and temperature inside the container during the process of gas accumulation.

At the first step, the simplified 3D physical model including the nozzle, an inlet pipe and the standard container is established as shown in Fig. 1.

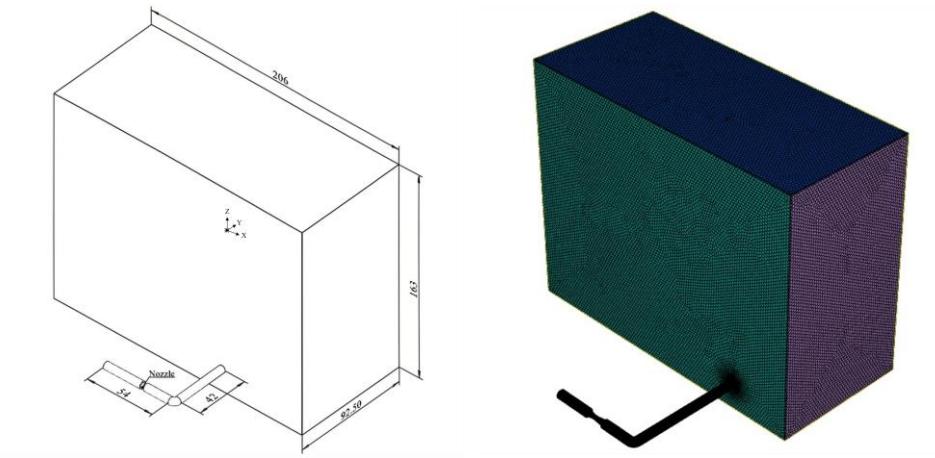


Fig. 1. Simplified 3D physical model of the gas flow verifier.

At the second step, the meshing of the 3D physical model and local grid refinement of the nozzle are implemented as exhibited in Fig. 2. To ensure the simulation accuracy and reduce calculation duration, the total mesh volume reaches 2.3 million according to grid independence verification.

Finally, the boundary conditions and initial conditions are set. The inlet boundary condition is set to flow inlet with the desired mass flow rate. The temperature of the wall is set constant with a value of 296K. The initial pressures are determined by the set value as shown in Table 1. To create an increasing flow rate, the pressure upstream the nozzle has to be increased, indicating an increasing critical pressure downstream the nozzle. Thus initial pressures varied and increased with flow rates for different flow rates. To ensure calculation accuracy and reduce calculation time, the time step is set to  $5 \times 10^{-4}$  s.

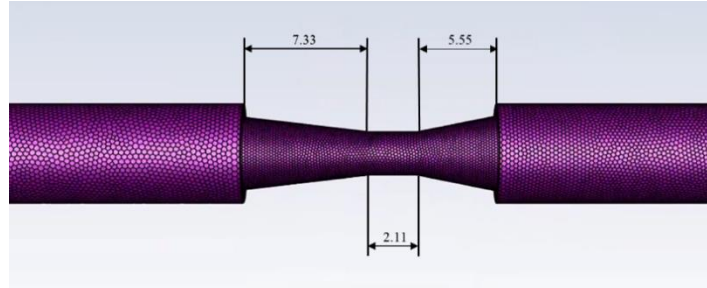


Fig. 1. Meshing of 3D physical model (left) and local grid refinement of the nozzle (right).

### 3. RESULTS AND DISCUSSION

#### 3.1. Experimental results

Real-time measurements of temperatures and pressures are implemented at  $N_2$  flow rate from 5~2850 sccm. As shown in Fig. 3, measured pressure remained stable before gas plenum, and increased linearly with time once the filling started. Time rate of pressure rise is taken as one of the input equations (2). From Wright et al. [4], temperature inside the container is spatial non-uniform due to flow work. However, the measured temperatures on the side and top walls of the standard container kept constant before and during the inflation, which cannot reflect non-uniform temperature distribution inside the container resulted by flow work. Thus, a 3D CFD simulation is needed.

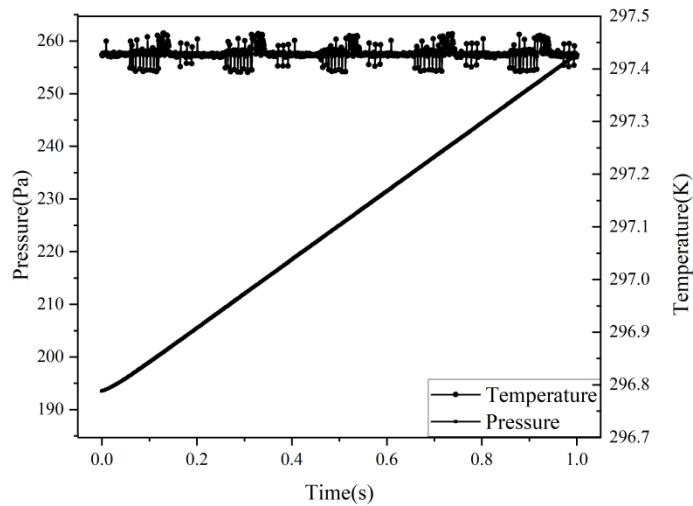


Fig. 2: Variation in tested pressure and temperature with time for  $N_2$  at a flow rate of 3000 sccm.

#### 3.2. Simulation results

Figs 4 and 5 display the temperature and pressure distribution inside the container at a state where average temperature of gas remains stable. From Fig. 6, the temperature inside the container is quite non-uniform. Local highest temperature can reach 311 K, while the temperature near the wall is the lowest with a value of 296 K. Otherwise, pressure inside the container is relatively uniform with the maximum pressure difference of 20 Pa.

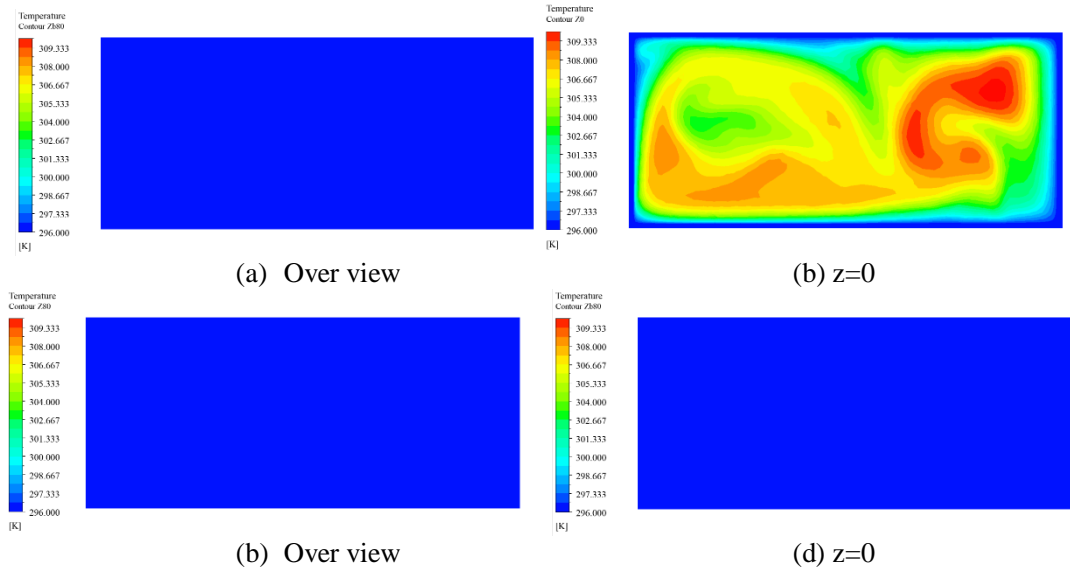


Fig. 3: Temperature distribution inside the container.

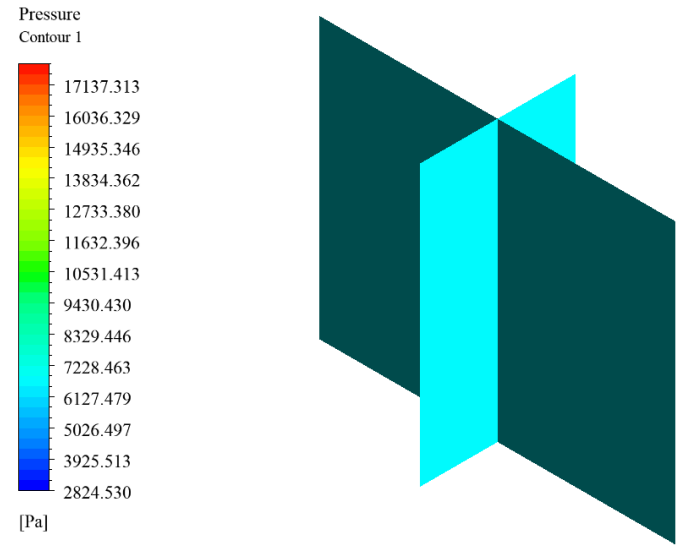


Fig. 4: Pressure distribution inside the container.

Fig. 6 exhibits the variation in simulated pressure with time for  $N_2$  at different flow rates. It can be observed that pressure increased linear with time and the rate of pressure rise increased with gas flow rate.

To validate the simulation, tested and simulated rates of pressure rise are compared. It can be seen from Fig. 7 that both tested and simulated rates of pressure rise experience a linear increase with gas flow rate. However, there exist some errors between simulated and tested rate of pressure rise.

Fig. 8 illustrates the variation in simulated average temperature with time for gas flow rate from 5 to 2850 sccm. The average gas temperature increased rapidly with time and then tended to be stable after 0.6 seconds, which was different from measured temperatures. Furthermore, average gas temperature with a stable value went up with a rise in gas flow rate.

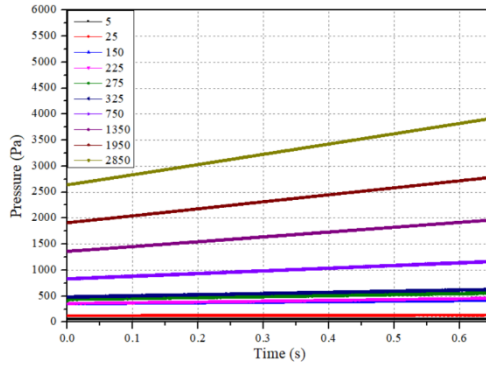


Fig. 5. Simulated pressure rising for N<sub>2</sub> at different flow rates.

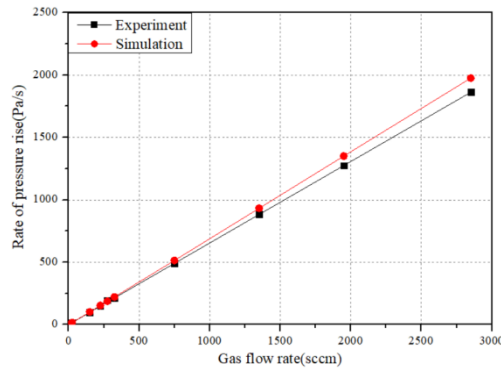


Fig. 6. Rate of pressure rise for N<sub>2</sub> at different flow rates.

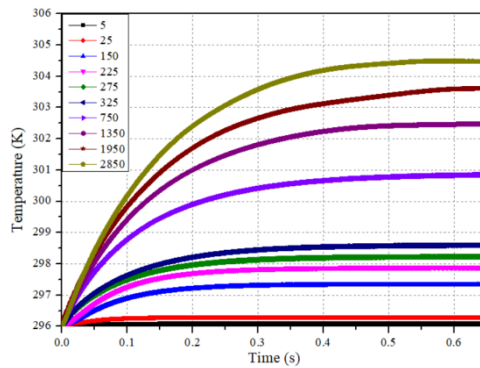


Fig. 7. Predicted temperature rise for N<sub>2</sub> at different flow rate.

The difference between average gas temperature with a state value and wall temperature is fitted as a function of flow rate as shown in Equations (3) and (4). Figs 9 and 10 display the variation in simulated temperature rise with N<sub>2</sub> flow rate from 5 to 2850 sccm. From Equation (3), fitting equation of temperature rise as a function of flow rate is linear for N<sub>2</sub> flow rate from 5 to 275 sccm:

$$\Delta T = 0.0079Q + 0.0345 \quad (3)$$

where  $\Delta T$  is the temperature rise, and  $Q$  is the flow rate of nitrogen (N<sub>2</sub>) in sccm (standard cubic centimeters per minute).

From Equation (4), fitting equation of temperature rise as a function of flow rate is cubic polynomial for N<sub>2</sub> flow rate from 325 to 2850 sccm:

$$\Delta T = 1.38 \times 10^{-10} Q^3 - 1.4 \times 10^{-6} Q^2 + 0.00539 Q + 1.17 \quad (4)$$

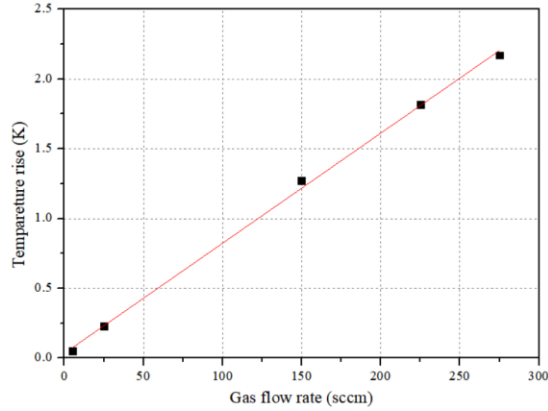


Fig. 8. Predicted temperature rise for N<sub>2</sub> range in 5~275 sccm.

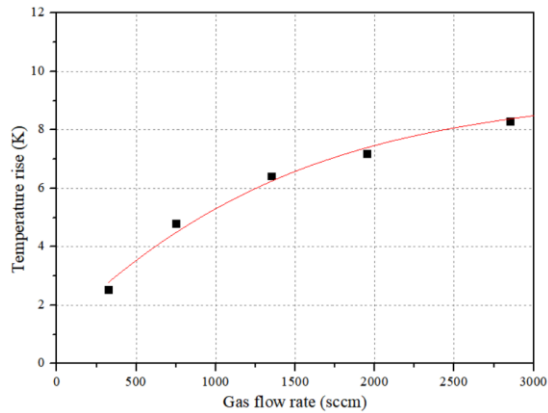


Fig. 9. Predicted temperature rise for N<sub>2</sub> range in 325~2850 sccm.

### 3.3. Gas flow rate calculation results

From Fig. 10, the average gas temperature tended to be independent with time 0.6 seconds after filling, thus, equation (2) can be simplified as follows:

$$\frac{dm}{dt} = \frac{V dp}{R_g T_g dt} \quad (5)$$

Basically, the gas flow rate is described by sccm in semiconductor process, thus equation (4) can be transformed into:

$$Q = \frac{6 \times 10^7 \times V dp}{\rho \cdot R_g T_g dt} \quad (6)$$

where  $\rho$  is the density of the gas at standard condition (101.325 kPa, 273.15K), and  $Q$  is the flow rate in sccm.

Based on simulation results, average gas temperature with a stable value can be calculated by the addition of wall temperature and the difference between stable average gas temperature and wall temperature:

$$Q = \frac{6 \times 10^7 \times V}{\rho \cdot R_g (T_w + \Delta T)} \frac{dp}{dt} \tag{7}$$

where  $T_w$  is the temperature of the container wall, and  $\Delta T$  is the difference between the steady average gas temperature and the container wall temperature.

If the difference between stable average gas temperature and wall temperature is neglected, an uncorrected gas flow rate can be obtained as well:

$$Q_0 = \frac{6 \times 10^7 \times V}{\rho \cdot R_g T_w} \frac{dp}{dt} \tag{8}$$

where  $Q_0$  is the uncorrected gas flow rate (in sccm).

Based on equations (7) and (8), the corrected and uncorrected gas flow rates were calculated and compared with reference value of the flow standard at flow rate from 5 to 2850 sccm. From Fig. 11, the maximum relative error of uncorrected gas flow rate reached as high as 2.8%. While the relative errors of corrected gas flow rate were within 0.5%, which meant that temperature correction improved the calculation accuracy of gas flow rate a great deal. It can be further observed that the effect of temperature correction was more remarkable at large flow rates due to significant flow work at high flow rates.

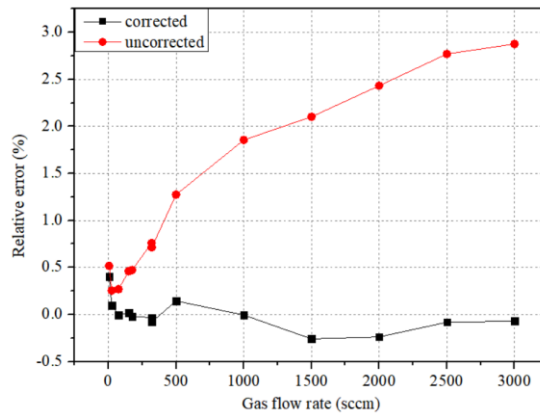


Fig. 10. Relative errors for corrected and uncorrected models.

#### 4. Conclusions

In this work, a dynamic temperature prediction method for the gas verifier based on the RoR dynamic pVTt method was carried out to obtain average gas temperature inside the standard container. Based on the state equation of idea gas, a model was developed to calculate gas flow rate. Several key findings are concluded as follows:

- 1) Based on the 3-D CFD simulation, spatial non-uniform temperature inside the standard container was obtained, which was further used to calculate average gas temperature inside the container.
- 2) Average gas temperature inside the standard container increased rapidly and remained stable 0.6 s after gas filling, indicating much shorter calibration time and higher calibration efficiency of RoR dynamic pVTt method compared to static pVTt method.
- 3) By temperature correction, maximum relative error of gas flow rates was reduced from 2.8% to 0.5%, improving the calculation accuracy of gas flow rate a great deal.

However, there exists some errors between simulated and tested rate of pressure rise. Thus, in the future work, accuracy of CFD simulation should be further improved and validated. So that the temperature prediction can be applied to other gases to validate the feasibility of the proposed model.

## Acknowledgements

This research was supported by Zhejiang Provincial Natural Science Foundation of China under Grant No. LQ24E060007, The Fundamental Research Funds of Zhejiang Province (No. 2022YW33), Zhejiang Provincial Administration for Market Regulation Science and Technology Plan(No. ZD2025005 and ZD2025006) and Open Foundation of the State Key Laboratory of Fluid Power and Mechatronic Systems (GZKF-202420).

## References

- [1] Ordu Mustafa. The role of semiconductors in the future of optical fibers[J]. *Frontiers in Physics*, 2023, 11.
- [2] M.S. Gaffney, C.M. Reaves, R.S. Smith, A.L.Holmes Jr., S.P.DenBaars. Control of III-V epitaxy in a metalorganic chemical vapor deposition process: impact of source flow control on composition and thickness. *Journal of Crystal Growth*, September 1996, 167(1-2): 8-16.
- [3] Verma G, Mondal K, Gupta A. Si-based MEMS resonant sensor: a review from microfabrication perspective[J]. *Microelectronics Journal*, 2021, 118: 105210.
- [4] Gaoming Zhang, Boxu Hui, Zhipeng Xu, Bin Zhou, Bengt Sundén, Zhen Cao. A review of calibration standards, devices and methods for gas flow in semiconductor manufacturing processes. *Flow Measurement and Instrumentation*, 2025, 101: 102753.
- [5] Wright, J.D., Nakao, S-I. Nakao, A.N. Johnson, M.R. Moldover. Gas flow standards and their uncertainty[J]. *Metrologia*, 2023, 60(1): 015002.
- [6] A.N. Johnson, J.D. Wright, M.R. Moldover, P.I. Espina. Temperature characterization in the collection tank of the NIST 26 m<sup>3</sup> pVTt gas flow standard[J]. *Metrologia*, 2003, 40(5): 211-216.
- [7] J.D. Wright, A.N. Johnson, M.R. Moldover, G.M. Kline. Errors in rate of rise gas flow measurements from flow work[C]. Queretaro, MX: Proceedings of the 10th International Symposium on Fluid Flow Measurement, 2018.
- [8] Žibret P, Bobovnik G, Kutin J. Correction for the temperature effects in a pVTt gas flow primary standard employing a dynamic method[J]. *Measurement*, 2023, 207: 112375.